Dynamics of a trapped Brownian particle in shear flows

Lukas Holzer,[1] Jochen Bammert,[1] Roland Rzehak,[2] and Walter Zimmermann[1]
[1]*Theoretische Physik I, Universität Bayreuth, D-95440 Bayreuth, Germany*
[2]*Störfallanalyse, Forschungszentrum Dresden, D-01328 Dresden, Germany*
(Received 16 November 2009; revised manuscript received 28 February 2010; published 20 April 2010)

The Brownian motion of a particle in a harmonic potential, which is simultaneously exposed either to a linear shear flow or to a plane Poiseuille flow is investigated. In the shear plane of both flows the probability distribution of the particle becomes anisotropic and the dynamics is changed in a characteristic manner compared to a trapped particle in a quiescent fluid. The particle distribution takes either an elliptical or a parachute shape or a superposition of both depending on the mean particle position in the shear plane. Simultaneously, shear-induced cross-correlations between particle fluctuations along orthogonal directions in the shear plane are found. They are asymmetric in time. In Poiseuille flow thermal particle fluctuations perpendicular to the flow direction in the shear plane induce a shift of the particle's mean position away from the potential minimum. Two complementary methods are suggested to measure shear-induced cross-correlations between particle fluctuations along orthogonal directions.

DOI: 10.1103/PhysRevE.81.041124 PACS number(s): 05.40.−a, 87.15.Ya, 83.50.Ax

I. INTRODUCTION

The Brownian motion of particles in a fluid is of central importance in chemical and biological physics as well as in material science and engineering [1–4]. Despite the long history of Brownian motion, especially in quiescent fluids, our understanding of thermally induced particle dynamics in flows is still far from complete.

Moreover, neutral colloidal particles moving relatively to each other interact via the fluid and these hydrodynamic interactions can cause a complex collective behavior [2–6]. In shear flows little is known about the dynamics of Brownian particles and the hydrodynamic interaction effects in spite of their fundamental relevance and importance in microfluidic applications. The Taylor dispersion [7] and fluid mixing issues [4,8] are well-known examples where fluctuations of particles and their hydrodynamic interaction effects in simple shear and Poiseuille flow play an important role. The interplay of shear gradients and thermal motion of polymers leads, even at low values of the Reynolds number, to the rich dynamics of polymers [9], the so-called molecular individualism [10]. Polymers tumbling in a shear flow cause elastic turbulence even in diluted polymer solutions [11] and spectacular mixing properties [8] in microchannels.

In shear flows, it is the contribution $(\mathbf{u}\cdot\boldsymbol{\nabla})\mathbf{u}$ of the flow field $\mathbf{u}(\mathbf{r})$ to the Navier-Stokes equation which causes interesting transient phenomena near the onset of turbulence [12], as well as amplifications of velocity fluctuations and their cross-correlations along and perpendicular to straight streamlines [13,14]. A cross-correlation is also expected between orthogonal particle fluctuations in the shear plane, because random jumps of a particle between neighboring streamlines of different velocity lead to a change in the particle's velocity and displacement along the streamlines, similar as via fluctuations. Nevertheless, there was no direct observation of these cross-correlations until recently [15]. Here we present the theoretical background for their determination.

The stochastic dynamics of free single spherical particles in linear shear flows have been studied in terms of the hydrodynamic fluctuation theory [16], and in combined Langevin and Fokker-Planck approaches, by taking inertia into account [17–19]. Even effects of nonequilibrium thermodynamics were included in Ref. [20]. Experiments for detecting shear-induced cross-correlations between perpendicular random displacements of free particles were described in Refs. [21,22]. Shear-induced cross-correlations between perpendicular fluid-velocity fluctuations and perpendicular fluctuations of particles are expected to be strongly asymmetric in time [13,18,23]. In dynamic light-scattering experiments certain aspects of this issue were observed indirectly [24], however, a direct measurement and characterization of related particle fluctuations in shear flows remained an open question.

Direct observations of particle fluctuations at the mesoscale became possible only quite recently by using optical tweezers. This rather young technique is a powerful experimental method for investigating the motion of a small number of particles [25–27], which contributes substantially to our understanding of the dynamics of particles and to a number of innovative applications. These include the inspiring studies on single polymers [28–35], the detection of anticorrelations between hydrodynamically interacting Brownian particles by Femto-Newton measurements [36], the propagation of hydrodynamic interactions [37], wall effects on Brownian motion [38,39], short-time inertial response of viscoelastic fluids [40], two-point microrheology [41], anomalous vibrational dispersion [42], particle sorting techniques [43–46], and a number of further investigations in microfluidics. The laser tweezer technique has also been applied to determine the force elongation relation of biopolymers [47] or the effective pair potential in colloidal suspensions [48].

Stochastic motions of a free particle moving along the streamlines of a sheared fluid and of a particle trapped in the minimum of a potential, while exposed to a shear flow, have common characteristic signatures. Since the trapped particles are more suited for a thorough statistical analysis of its Brownian dynamics, we present calculations for particles trapped by a harmonic potential and exposed to either a linear shear flow or to a plane Poiseuille flow. Our analytical

results show that shear flow causes characteristic signatures in the time dependence of the cross-correlation between particle displacements along orthogonal directions in the shear plane as well as an inclined elliptical particle distribution. Part of these results have already been applied and confirmed in a recent experimental study [15].

For our calculations, we utilize a Langevin model for the particle motion, where stochastic forces with different statistical properties may be used. Stochastic forces acting on suspended Brownian particles are caused by velocity fluctuations of the surrounding fluid. In a quiescent fluid the fluctuations of orthogonal velocity components are uncorrelated in the bulk [49]. Assuming such uncorrelated fluid-velocity fluctuations, and therefore uncorrelated stochastic forces in the particle Langevin model, we show how shear flow induces cross-correlations between particle fluctuations along orthogonal directions. Conversely, we show how the amplitudes of the stochastic forces acting on the particle can be determined by measuring the static correlations of the particle fluctuations.

In Sec. II the model equations of the Brownian particle motion and their formal analytical solutions are presented. The static correlation functions for the particle's position and velocity fluctuations are derived in Sec. III, where also the corresponding distributions are calculated in terms of the static correlations and under the assumption of Gaussian particle fluctuations. In addition, the ratio between the principal axes of both distributions are determined as well as the angle enclosed by each major axis and the flow direction. In Poiseuille flow the second derivative of the flow profile, as well as the fluctuations perpendicular to the flow lines, cause a shift of the particle's mean position in the potential via $\Delta\mathbf{u}(\mathbf{r}) \neq 0$. The latter contribution is usually not taken into account, if the effective particle radius is determined via Faxén's law from the particle displacement. In Sec. IV we present and discuss these results for the special cases of linear shear flow and plane Poiseuille flow. In addition, we compare the analytical results with numerical simulations of the Langevin equation given in Sec. II and we suggest experiments to measure some of the flow-induced effects determined in this work. The article closes with a discussion and possible further applications in Sec. V.

II. EQUATIONS OF MOTION AND THEIR SOLUTIONS

We consider a Brownian particle of mass m and effective radius R suspended at the position $\mathbf{r}=(x,y,z)$ in a flow field with parallel streamlines in the x-direction, $\mathbf{u}(\mathbf{r})=u_x(y)\hat{\mathbf{e}}_x$. We assume a velocity field

$$u_x(y) = (a + by + cy^2), \tag{1}$$

which corresponds for $b=c=0$ to a uniform flow, for $a=c=0$ to a linear shear flow with shear rate b, and for $c=-\frac{a}{l^2}$, $b=0$ to a plane Poiseuille flow between two parallel walls at a distance $2l$. The particle is trapped by a harmonic potential with its minimum at $\mathbf{r}_0=(x_0,y_0,z_0)=(0,0,0)$,

$$U(\mathbf{r}) = \frac{k}{2}\mathbf{r}^2. \tag{2}$$

The resulting linear restoring force is given by

$$\mathbf{F}^p = -\nabla U = -k\mathbf{r}, \tag{3}$$

in terms of the force constant k. Such a potential acting on a colloidal particle may be realized by an optical tweezer [25].

A particle moving with the speed $\mathbf{v}=\dot{\mathbf{r}}$ in a flow of velocity $\mathbf{u}$ experiences, according to Stokes' law, a hydrodynamic drag force $\mathbf{F}^h=6\pi\eta R(\mathbf{u}-\mathbf{v})$ proportional to the effective radius R, to the shear viscosity η and to the difference $\mathbf{u}-\mathbf{v}$ between the velocity of the particle and the local flow velocity [49,50]. If the flow velocity $\mathbf{u}(\mathbf{r})$ is a nonlinear function of the spatial coordinates, as in the case of a plane Poiseuille flow in Eq. (1), one has according to Faxén's theorems [51] an additional contribution to the drag force. This contribution includes the Laplacian of the velocity field and has in terms of the Stokes friction coefficient, $\zeta=6\pi\eta R$, the form

$$\mathbf{F}^h = -\zeta\left(\dot{\mathbf{r}} - \mathbf{u}(\mathbf{r}) - \frac{R^2}{6}\Delta\mathbf{u}(\mathbf{r})\right). \tag{4}$$

The Laplacian of the flow field in Eq. (1), with the abbreviation $\bar{a}=a+\frac{R^2}{3}c$, gives the following expression for the hydrodynamic drag force,

$$\mathbf{F}^h = -\zeta\dot{\mathbf{r}} + \zeta(\bar{a} + by + cy^2)\hat{\mathbf{e}}_x. \tag{5}$$

The stochastic motion of a Brownian particle is caused by the fluctuations $\tilde{\mathbf{u}}$ of the fluid-velocity field $\mathbf{u}(\mathbf{r},t)$ [52]. The effects of $\tilde{\mathbf{u}}$ on a particle can be taken into account in a Langevin model by a random force $\mathbf{F}^b(t)$. In uniform flows, namely with $b=c=0$ in Eq. (1), the cross-correlations of the velocity fluctuations of the fluid, $\langle\tilde{u}_i\tilde{u}_j\rangle$, lead to a vanishing cross-correlation of the random forces, $\langle F_i^b F_j^b\rangle=0$, $(i\neq j)$. The shear-induced contributions to $\tilde{u}_i$ and F_i^b are a matter of current research [13,14].

In our model we assume a Gaussian distribution of $\mathbf{F}^b(t)$ with vanishing correlation time and mean value

$$\langle F_i^b(t)\rangle = 0,$$

$$\langle F_i^b(t)F_j^b(t')\rangle = f_{ij}\delta(t-t') \quad \text{and} \quad i,j \in x,y,z. \tag{6}$$

For the moment we leave the fluctuation matrix f_{ij} unspecified, except to note that, according to time-translation and time-reversal invariance, it is symmetric. In uniform flows, namely, with $b=c=0$ in Eq. (1), the matrix f_{ij} is diagonal with $f_{ii}=2k_BT\zeta$ [53] as mentioned before, whereas in a shear flow the magnitude of the nondiagonal elements of f_{ij} depends on the shear rate, but shear-induced contributions are expected to be small [13,16,23]. However, we allow nondiagonal elements of f_{ij} for the moment to show in Sec. IV how these nondiagonal elements may be determined by measurements of the velocity fluctuations of the particle.

The net force acting on the particle,

$$\mathbf{F} = \mathbf{F}^h + \mathbf{F}^p + \mathbf{F}^b(t), \tag{7}$$

together with Newton's law gives the Langevin equations of motion for the translational degrees of freedom of the particle

$$m\ddot{x} = -\zeta\dot{x} - kx + \zeta(\bar{a} + by + cy^2) + F_x^b(t), \tag{8a}$$

$$m\ddot{y} = -\zeta\dot{y} - ky + F_y^b(t), \tag{8b}$$

$$m\ddot{z} = -\zeta\dot{z} - kz + F_z^b(t). \tag{8c}$$

Introducing the vectors $\mathbf{X}=(x,v_x)$, $\mathbf{Y}=(y,v_y)$, and $\mathbf{Z}=(z,v_z)$ one may express the second order differential Eq. (8) in terms of a system of coupled first-order equations

$$\dot{\mathbf{X}} = \mathrm{L}\mathbf{X} + \frac{F_x^b(t)}{m}\hat{\mathbf{e}}_v + 2\beta(\bar{a} + by + cy^2)\hat{\mathbf{e}}_v, \tag{9a}$$

$$\dot{\mathbf{Y}} = \mathrm{L}\mathbf{Y} + \frac{F_y^b(t)}{m}\hat{\mathbf{e}}_v, \tag{9b}$$

$$\dot{\mathbf{Z}} = \mathrm{L}\mathbf{Z} + \frac{F_z^b(t)}{m}\hat{\mathbf{e}}_v. \tag{9c}$$

Herein we have introduced the matrix

$$\mathrm{L} = \begin{pmatrix} 0 & 1 \\ -\omega^2 & -2\beta \end{pmatrix}, \tag{10}$$

the damping constant $\beta=\frac{\zeta}{2m}$, the squared frequency $\omega^2=\frac{k}{m}$ and the velocity unit-vector $\hat{\mathbf{e}}_v=(0,1)$. The rotational motion of the particle, which may provide further corrections to the leading order fluctuation effects discussed here, is not taken into account in this work.

The general solutions of the equations of motion (9) in terms of the initial conditions $\mathbf{X}(0)$, $\mathbf{Y}(0)$, and $\mathbf{Z}(0)$ are given by

$$\mathbf{X}(t) = e^{\mathrm{L}t}\mathbf{X}(0) + \int_0^t d\tau e^{\mathrm{L}(t-\tau)}\frac{F_x^b(\tau)}{m}\hat{\mathbf{e}}_v + 2\beta\int_0^t d\tau e^{\mathrm{L}(t-\tau)}(\bar{a} + by + cy^2)\hat{\mathbf{e}}_v, \tag{11a}$$

$$\mathbf{Y}(t) = e^{\mathrm{L}t}\mathbf{Y}(0) + \int_0^t d\tau e^{\mathrm{L}(t-\tau)}\frac{F_y^b(\tau)}{m}\hat{\mathbf{e}}_v, \tag{11b}$$

$$\mathbf{Z}(t) = e^{\mathrm{L}t}\mathbf{Z}(0) + \int_0^t d\tau e^{\mathrm{L}(t-\tau)}\frac{F_z^b(\tau)}{m}\hat{\mathbf{e}}_v. \tag{11c}$$

This system of coupled equations is the starting point of the following analysis, where the statistical properties of the particle's motion are characterized by the correlations of its position and velocity.

III. DISTRIBUTION FUNCTIONS AND STATIC CORRELATIONS

By taking the averages of Eq. (11) and using the vanishing mean of the stochastic forces in Eq. (6) we see that the mean velocity of a particle in a harmonic potential vanishes, $\langle\mathbf{v}\rangle=0$. In the case $\mathbf{r}_0=0$ the mean value of the deviations of the particle's position from the potential minimum in the directions perpendicular to the flow vanish too, $\langle y\rangle=\langle z\rangle=0$. However, the mean particle displacement in the direction of the flow given by Eq. (1) is nonzero

$$\langle x\rangle = \frac{\zeta}{k}\bar{a} + \frac{f_{yy}}{2k^2}c. \tag{12}$$

This equation is discussed in more detail in Sec. IV for specific flows. Since the spring constant k of the potential enters in different powers in Eq. (12), this formula might be employed for the experimental determination of the effective fluctuation magnitude f_{yy}.

With a combination of the coordinates of the particle and its velocities to a single six-dimensional vector, $\mathbf{q}=(\mathbf{r},\mathbf{v})=(x,y,z,v_x,v_y,v_z)$, the probability distribution function of the particle, $\mathcal{P}(\mathbf{q})$, may be formulated in a compact form in terms of the deviations $\tilde{\mathbf{q}}=\mathbf{q}-\langle\mathbf{q}\rangle=(\tilde{x},\tilde{y},\tilde{z},\tilde{v}_x,\tilde{v}_y,\tilde{v}_z)$ from the mean value $\langle\mathbf{q}\rangle$. If the fluctuations $\tilde{\mathbf{q}}$ are linear functions of Gaussian distributed stochastic forces, which is the case for uniform and linear shear flows, they can be expected to be themselves Gaussian variables [54] and can be described by a Gaussian distribution as follows:

$$\mathcal{P}(\tilde{\mathbf{q}}) = \frac{1}{\sqrt{(2\pi)^6\det(\mathrm{C})}}\exp\left(-\frac{1}{2}\tilde{\mathbf{q}}^T\mathrm{C}^{-1}\tilde{\mathbf{q}}\right). \tag{13}$$

Here the covariance matrix $\mathrm{C}=\langle\tilde{\mathbf{q}}\tilde{\mathbf{q}}^T\rangle$ is used, which includes second-order moments for the coordinates and the velocities at equal times (static correlations). The magnitudes of the elements C_{ij} depend on the correlation amplitudes of the stochastic forces, f_{ij}, and can be measured in experiments. Consequently, one may reconstruct the stochastic forces from the measurements, as discussed later.

For Poiseuille flow the relations between particle fluctuations and stochastic forces are nonlinear due to the contribution $\propto cy^2$ in Eq. (11a). Therefore, the particle distribution $\mathcal{P}(\tilde{\mathbf{q}})$ is not necessarily Gaussian. However, in the course of this work we use the formula in Eq. (13) also for particles in a potential, which are exposed to a Poiseuille flow, but with the covariance matrix C_{ij} now determined in terms of the parameters for the Poiseuille flow. The validity of this heuristic approach will be tested later in Sec. IV B by numerical simulations.

A. Covariance matrix and angular momentum

The covariance matrix C consists of four 3×3 submatrices

$$\mathrm{C} = \begin{pmatrix} \mathrm{C}_{rr} & \mathrm{C}_{rv} \\ \mathrm{C}_{vr} & \mathrm{C}_{vv} \end{pmatrix}, \tag{14}$$

that describe the autocorrelation for the positions C_{rr} and velocities C_{vv} and their cross-correlations C_{vr} and C_{rv} at equal times. The matrices

$$\mathrm{C}_{rr} = \begin{pmatrix} \langle \tilde{x}^2 \rangle & \langle \tilde{x}\tilde{y} \rangle & 0 \\ \langle \tilde{y}\tilde{x} \rangle & \langle \tilde{y}^2 \rangle & 0 \\ 0 & 0 & \langle \tilde{z}^2 \rangle \end{pmatrix}, \tag{15a}$$

$$\mathrm{C}_{vv} = \begin{pmatrix} \langle \tilde{v}_x^2 \rangle & \langle \tilde{v}_x\tilde{v}_y \rangle & 0 \\ \langle \tilde{v}_y\tilde{v}_x \rangle & \langle \tilde{v}_y^2 \rangle & 0 \\ 0 & 0 & \langle \tilde{v}_z^2 \rangle \end{pmatrix}, \tag{15b}$$

$$\mathrm{C}_{rv} = \mathrm{C}_{vr}^T = \begin{pmatrix} 0 & \langle \tilde{x}\tilde{v}_y \rangle & 0 \\ \langle \tilde{y}\tilde{v}_x \rangle & 0 & 0 \\ 0 & 0 & 0 \end{pmatrix}, \tag{15c}$$

may be calculated in terms of the expressions given by Eq. (11).

Under the Gaussian assumption, the four-point correlations of the stochastic forces, which occur due to the quadratic contribution y^2 of the flow in Eq. (11a), can be decomposed into two-point correlation functions according to Wick's theorem [54]:

$$\begin{aligned} \langle F_i^b(t_1)F_j^b(t_2)F_k^b(t_3)F_l^b(t_4)\rangle = {} & f_{ij}f_{kl}\delta(t_2-t_1)\delta(t_4-t_3) \\ & + f_{ik}f_{jl}\delta(t_3-t_1)\delta(t_4-t_3) \\ & + f_{il}f_{jk}\delta(t_4-t_1)\delta(t_3-t_2). \end{aligned} \tag{16}$$

Introducing the relaxation time of the particle in a harmonic potential

$$\tau_p = \frac{\zeta}{k}, \tag{17}$$

the nonzero components of the covariance matrices may be written in terms of the amplitudes of the stochastic forces and the flow parameters by the following set of equations:

$$\langle \tilde{v}_y^2 \rangle = \frac{1}{4}\frac{f_{yy}}{m^2\beta}, \quad \langle \tilde{y}^2 \rangle = \frac{\langle \tilde{v}_y^2 \rangle}{\omega^2}, \tag{18a}$$

$$\langle \tilde{v}_z^2 \rangle = \frac{1}{4}\frac{f_{zz}}{m^2\beta}, \quad \langle \tilde{z}^2 \rangle = \frac{\langle \tilde{v}_z^2 \rangle}{\omega^2}, \tag{18b}$$

$$\langle \tilde{v}_x\tilde{v}_y \rangle = \langle \tilde{v}_y\tilde{v}_x \rangle = \frac{1}{4}\frac{f_{xy}}{m^2\beta}, \tag{18c}$$

$$\langle \tilde{x}\tilde{y} \rangle = \langle \tilde{y}\tilde{x} \rangle = \frac{\langle \tilde{v}_x\tilde{v}_y \rangle}{\omega^2} + \frac{1}{2}b\tau_p\langle \tilde{y}^2 \rangle, \tag{18d}$$

$$\langle \tilde{x}\tilde{v}_y \rangle = -\langle \tilde{y}\tilde{v}_x \rangle = -\frac{b}{2}\langle \tilde{y}^2 \rangle, \tag{18e}$$

$$\langle \tilde{v}_x^2 \rangle = \frac{1}{4}\frac{f_{xx}}{m^2\beta} + \frac{1}{2}b^2\langle \tilde{y}^2 \rangle + \frac{8c^2\tau_p^2\omega^2}{3(1+2\tau_p^2\omega^2)}\langle \tilde{y}^2 \rangle^2, \tag{18f}$$

$$\langle \tilde{x}^2 \rangle = \frac{\langle \tilde{v}_x^2 \rangle}{\omega^2} + \tau_p b\langle \tilde{x}\tilde{y} \rangle + \frac{2}{3}\tau_p^2 c^2\langle \tilde{y}^2 \rangle^2. \tag{18g}$$

The nondiagonal elements of C_{vv}, namely, the correlations of the velocity fluctuations of the particle, $\langle \tilde{v}_x\tilde{v}_y \rangle$ and $\langle \tilde{v}_y\tilde{v}_x \rangle$, are directly proportional to the amplitude f_{xy} of the fluctuations given by Eq. (6). In contrast to this result for a fluctuating particle in a potential, one finds for a free particle in shear flow finite values for the cross-correlations $\langle \tilde{v}_x\tilde{v}_y \rangle$ and $\langle \tilde{v}_y\tilde{v}_x \rangle$ even in the case $f_{xy}=0$ [18]. However, as shown appendix A, in the presence of a harmonic potential these correlations decay on a time scale $1/(2\beta)$, which is very short for an overdamped particle motion. In the case of a weak laser tweezer potential the particle relaxation time $\tau_p=\zeta/k$ becomes rather large and one obtains according to Eqs. (A8) and (A10) for $f_{xy}=0$ a contribution to the velocity correlation $\langle \tilde{v}_x(t)\tilde{v}_y(t) \rangle \propto \exp[-2t/\tau_p]f_{yy}$, which decays slowly and gives in the limit of a vanishing potential ($k \to 0, \tau_p \to \infty$) a constant contribution to the velocity-velocity correlation, which agrees with that in Ref. [18] for a free particle, cf. Appendix A. Therefore, finite values of $\langle \tilde{v}_x\tilde{v}_y \rangle$ and $\langle \tilde{v}_y\tilde{v}_x \rangle$ measured for particles trapped in a potential are a direct indication of cross-correlations of the stochastic forces along orthogonal directions, $\langle F_x^b F_y^b \rangle \neq 0$.

For $b \neq 0$ the contributions to the nondiagonal elements $\langle \tilde{x}\tilde{y} \rangle$ and $\langle \tilde{y}\tilde{x} \rangle$ of the positional correlations C_{rr}, which are related to $f_{xy} \propto b$, are expected to be small [14,23]. For this reason f_{xy} is neglected in the following. Both positional cross-correlations $\langle \tilde{x}\tilde{y} \rangle$ and $\langle \tilde{y}\tilde{x} \rangle$ are proportional to the local shear rate b and to the fluctuation strength f_{yy} in the y direction, cf. Eq. (18d).

The autocorrelation of the velocity fluctuations $\langle \tilde{v}_x^2 \rangle$ in the flow direction includes several contributions. It depends on the shear rate, the second derivative of the flow and the fluctuation strength f_{xx} and f_{yy}. The cross-correlations between velocity and position appear only in the shear plane and they are proportional to the local shear rate.

The submatrices C_{vr} and C_{rv}, describing the cross-correlations between the positional and the velocity fluctuations, are related to the mean angular momentum of the particle

$$\langle (m\mathbf{r} \times \mathbf{v})_z \rangle = m\langle \tilde{x}\tilde{v}_y - \tilde{y}\tilde{v}_x \rangle = -mb\langle \tilde{y}^2 \rangle. \tag{19}$$

B. Distribution of position and velocity

Integrating the particle distribution function $\mathcal{P}(\tilde{\mathbf{q}})$ in Eq. (13) with respect to its velocity degrees of freedom one obtains the particle's positional distribution function $\mathcal{P}(\tilde{\mathbf{r}})$, which may be expressed in terms of the covariance matrix C_{rr} as follows:

$$\mathcal{P}(\tilde{\mathbf{r}}) = \int d\tilde{\mathbf{v}}\mathcal{P}(\tilde{\mathbf{q}}) = \frac{1}{\sqrt{(2\pi)^3 \det(\mathrm{C}_{rr})}} \exp\left(-\frac{1}{2}\tilde{\mathbf{r}}^T \mathrm{C}_{rr}^{-1}\tilde{\mathbf{r}}\right). \tag{20}$$

A sketch of the distribution $\mathcal{P}(\tilde{\mathbf{r}})$ is shown in Fig. 1 for a linear shear flow $b \neq 0$ and $a=c=0$. The nondiagonal elements of the symmetric matrix C_{rr}, cf. Eq. (15a) and (18),

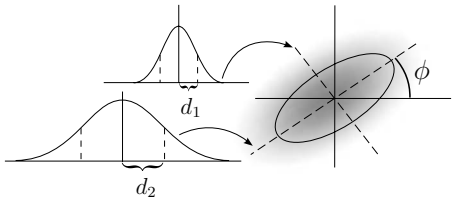

FIG. 1. The elliptical particle distribution in the xy shear plane is sketched for a nonzero shear rate. d_1 and d_2 are the two principal axes of an ellipse along which $\mathcal{P}(\tilde{\mathbf{r}})$ is constant. The Gaussian profiles along the two principal axes are also indicated.

describe the cross-correlations of the particle fluctuations in the x and y direction and therefore the deviation of $\mathcal{P}(\tilde{\mathbf{r}})$ from a spherically symmetric distribution to an ellipsoidal one in the shear plane. The principal axes of the particle's positional distribution are given by the eigenvectors $\mathbf{w}_{p;1,2,3}$ of the corresponding eigenvalues $c_{p;1,2,3}$ of the matrix C_{rr}.

In the z-direction one has $c_{p;3}=\langle\tilde{z}^2\rangle$ and $\mathbf{w}_{p;3}=(0,0,1)$. For the other two directions in the xy shear plane one obtains

$$c_{p;1,2}=\frac{1}{2}(\langle\tilde{x}^2\rangle+\langle\tilde{y}^2\rangle)\pm\frac{1}{2}\sqrt{4\langle\tilde{x}\tilde{y}\rangle^2+(\langle\tilde{x}^2\rangle-\langle\tilde{y}^2\rangle)^2},$$

$$\mathbf{w}_{p;1}=\left(\frac{c_{p;1}-\langle\tilde{y}^2\rangle}{\langle\tilde{x}\tilde{y}\rangle},1,0\right),$$

$$\mathbf{w}_{p;2}=\frac{\langle\tilde{x}\tilde{y}\rangle}{|\langle\tilde{x}\tilde{y}\rangle|}\left(-1,\frac{c_{p;1}-\langle\tilde{y}^2\rangle}{\langle\tilde{x}\tilde{y}\rangle},0\right). \tag{21}$$

With the orthogonal transformation matrix

$$\mathrm{D}=(\mathbf{w}_{p;1},\mathbf{w}_{p;2},\mathbf{w}_{p;3}), \tag{22}$$

the $\tilde{\mathbf{r}}$-dependence of the exponential function (20) can be rewritten as follows:

$$-\frac{1}{2}\tilde{\mathbf{r}}^T\mathrm{C}_{rr}^{-1}\tilde{\mathbf{r}}=-\frac{1}{2}(\mathrm{D}^T\tilde{\mathbf{r}})^T\mathrm{diag}(c_{p;1}^{-1},c_{p;2}^{-1},c_{p;3}^{-1})(\mathrm{D}^T\tilde{\mathbf{r}}). \tag{23}$$

The eigenvalues $c_{p;1}$ and $c_{p;2}$ determine the length of the principal axes $d_{p;1,2}=\sqrt{c_{p;1,2}}$ along the directions $\mathbf{w}_{p;1}$ and $\mathbf{w}_{p;2}$ of an ellipse, where the longer one is rotated counterclockwise with respect to the x-axis by an angle ϕ_p, which is given by the expression

$$\tan\phi_p=\frac{\langle\tilde{x}\tilde{y}\rangle}{c_{p,1}-\langle\tilde{y}^2\rangle}=\frac{1}{2}\left[\frac{\langle\tilde{x}\tilde{y}\rangle}{|\langle\tilde{x}\tilde{y}\rangle|}\sqrt{4+\left(\frac{\langle\tilde{x}^2\rangle-\langle\tilde{y}^2\rangle}{\langle\tilde{x}\tilde{y}\rangle}\right)^2}-\left(\frac{\langle\tilde{x}^2\rangle-\langle\tilde{y}^2\rangle}{\langle\tilde{x}\tilde{y}\rangle}\right)\right]. \tag{24}$$

The ratio between the minor and the major axis is given by

$$V_p:=\sqrt{\frac{c_{p;2}}{c_{p;1}}}=\left(\frac{\langle\tilde{x}^2\rangle+\langle\tilde{y}^2\rangle-\sqrt{4\langle\tilde{x}\tilde{y}\rangle^2+(\langle\tilde{x}^2\rangle-\langle\tilde{y}^2\rangle)^2}}{\langle\tilde{x}^2\rangle+\langle\tilde{y}^2\rangle+\sqrt{4\langle\tilde{x}\tilde{y}\rangle^2+(\langle\tilde{x}^2\rangle-\langle\tilde{y}^2\rangle)^2}}\right)^{1/2}. \tag{25}$$

Analogous to the particle distribution given above, one can also derive an expression for the probability distribution $\mathcal{P}(\tilde{\mathbf{v}})$ of the particle's velocity, which is obtained by integrating out the positional degrees of freedom in Eq. (13)

$$\mathcal{P}(\tilde{\mathbf{v}})=\int d\tilde{\mathbf{r}}\mathcal{P}(\tilde{\mathbf{r}},\tilde{\mathbf{v}})=\frac{1}{\sqrt{(2\pi)^3\det(\mathrm{C}_{vv})}}\exp\left(-\frac{1}{2}\tilde{\mathbf{v}}^T\mathrm{C}_{vv}^{-1}\tilde{\mathbf{v}}\right). \tag{26}$$

The eigenvalues $c_{v;1,2,3}$ and eigenvectors $\mathbf{w}_{v;1,2,3}$ of C_{vv} are determined in a similar manner as for C_{rr}. Again the eigenvalue $c_{v;3}=\langle\tilde{v}_z^2\rangle$ and the principal axis $\mathbf{w}_{v;3}=(0,0,1)$ perpendicular to the shear plane are obvious. The remaining two eigenvalues and eigenvectors are

$$c_{v;1,2}=\frac{1}{2}(\langle\tilde{v}_x^2\rangle+\langle\tilde{v}_y^2\rangle)\pm\frac{1}{2}\sqrt{4\langle\tilde{v}_x\tilde{v}_y\rangle^2+(\langle\tilde{v}_x^2\rangle-\langle\tilde{v}_y^2\rangle)^2},$$

$$\mathbf{w}_{v;1}=\left(\frac{c_{v;1}-\langle\tilde{v}_y^2\rangle}{\langle\tilde{v}_x\tilde{v}_y\rangle},1,0\right), \tag{27}$$

$$\mathbf{w}_{v;2}=\frac{\langle\tilde{v}_x\tilde{v}_y\rangle}{|\langle\tilde{v}_x\tilde{v}_y\rangle|}\left(-1,\frac{c_{v;1}-\langle\tilde{v}_y^2\rangle}{\langle\tilde{v}_x\tilde{v}_y\rangle},0\right). \tag{28}$$

They have the same structure like those for the covariance matrix C_{rr}. However, while the nondiagonal elements of C_{rr} are directly proportional to the local shear rate b, the nondiagonal elements of C_{vv} and therefore the angle enclosed between the principal axis of the distribution of the velocity fluctuations and the x axis,

$$\tan\phi_v=\frac{\langle\tilde{v}_x\tilde{v}_y\rangle}{c_{v,1}-\langle\tilde{v}_y^2\rangle}=\frac{1}{2}\left[\frac{\langle\tilde{v}_x\tilde{v}_y\rangle}{|\langle\tilde{v}_x\tilde{v}_y\rangle|}\sqrt{4+\left(\frac{\langle\tilde{v}_x^2\rangle-\langle\tilde{v}_y^2\rangle}{\langle\tilde{v}_x\tilde{v}_y\rangle}\right)^2}-\left(\frac{\langle\tilde{v}_x^2\rangle-\langle\tilde{v}_y^2\rangle}{\langle\tilde{v}_x\tilde{v}_y\rangle}\right)\right], \tag{29}$$

depends only weakly on the local shear rate, since the contribution of b to the shear-induced cross-correlation f_{xy} is small in magnitude, compared to f_{ii} [14,23]. From a measurement of the distribution of the particle's velocity one may calculate the eigenvalues $c_{v;1,2}$ and the angle ϕ_v, which may enable the determination of the stochastic force correlations f_{xx}, f_{yy}, and f_{xy}.

The mean kinetic energy of a trapped particle in shear flow is composed of two contributions, one induced by the distribution of the fluctuations and an additional one by virtue of the rotational part of the flow

$$E_{kin}=\frac{m}{2}\langle\tilde{v}_x^2+\tilde{v}_y^2+\tilde{v}_z^2\rangle=\frac{1}{4}\frac{f_{xx}+f_{yy}+f_{zz}}{m^2\beta}+\frac{b^2}{2}\langle\tilde{y}^2\rangle+\frac{8}{3}c^2\frac{\tau_p^2\omega^2}{1+2\tau_p^2\omega^2}\langle\tilde{y}^2\rangle^2. \tag{30}$$

If the correlations of the stochastic forces are assumed to be independent of the flow, the mean energy of the particle will be increased by the flow, since all terms in this equation are positive. But without knowing the explicit expressions for the force correlations, it is not clear how the energy is really changed. Recent calculations show that the mean kinetic energy of a fluid without an immersed particle increases in a

shear flow [55,56]. This indicates that the stochastic forces and the particle's mean energy, Eq. (30), may be amplified as well.

IV. RESULTS FOR SPECIFIC FLOWS

The results concerning the effects of a linear shear and a plane Poiseuille flow on the Brownian motion of a particle in a harmonic potential are presented in this section. Namely, the properties of the correlation functions and the particle's distribution are analyzed as a function of the flow parameters. They share common trends for both flows but there are also some characteristic differences, which are described in this section.

A. Linear shear flow

If the center of the harmonic potential at $\mathbf{r}_0=(0,y_0,0)$ does not coincide with the center of the linear shear flow of shear rate $\dot{\gamma}$, we may insert in Eq. (1) $y=y_0+\tilde{y}$, where $\tilde{y}$ describes the deviation from y_0. Consequently, in terms of the coordinates $\tilde{y}$, the three coefficients in Eq. (1) take the following form

$$b=\dot{\gamma}, \quad a=\bar{a}=\dot{\gamma}y_0 \quad \text{and} \quad c=0. \tag{31}$$

In the case $y_0\neq 0$ the flow velocity has a finite value at the center of the trap resulting in a nonzero mean position of the particle in flow direction, which is given via Eq. (12) by the formula

$$\langle x\rangle=\dot{\gamma}\tau_p y_0. \tag{32}$$

With the identifications (31) the elements of the covariance matrix C for the particle fluctuations around the potential minimum may be determined for a linear shear flow by Eq. (18) in terms of the noise amplitudes f_{xx}, f_{xy}, and f_{yy}.

An interesting question is how to detect the noise amplitudes f_{ij} in terms of the measured autocorrelations and cross-correlations of the particle's position- and velocity fluctuations. According to Eq. (18c) there is a direct relation between the velocity correlation $\langle\tilde{v}_x\tilde{v}_y\rangle$ and the noise magnitude f_{xy}. Therefore, a direct measurement of this velocity correlation, if experimentally possible, would give f_{xy}, or, the other way around, a nonzero value of $f_{xy}\neq 0$ is required in order to obtain nonzero values of the cross-correlations between these orthogonal velocity components.

As already mentioned in the introduction, it is favorable to investigate the particle fluctuations around a potential minimum rather than those of free particles since trapped particles can be investigated over a long period of time, as demonstrated by several experiments, see e. g., Ref. [36]. This opens the opportunity for the determination of the magnitudes of the noise f_{ij} in terms of the positional fluctuations via Eq. (18), which in the case of a linear shear flow take the following explicit form

$$f_{yy}=2k\zeta\langle\tilde{y}^2\rangle, \tag{33a}$$

$$f_{xy}=2k\zeta\left(\langle\tilde{x}\tilde{y}\rangle-\frac{1}{2}\dot{\gamma}\tau_p\langle\tilde{y}^2\rangle\right), \tag{33b}$$

$$f_{xx}=2k\zeta\left(\langle\tilde{x}^2\rangle-\frac{1}{2}\frac{\dot{\gamma}^2}{\omega^2}\langle\tilde{y}^2\rangle-\dot{\gamma}\tau_p\langle\tilde{x}\tilde{y}\rangle\right). \tag{33c}$$

In the case of isotropic stochastic forces with negligible cross-correlations, $f_{xx}=f_{yy}$ and $f_{xy}\propto\langle\tilde{v}_x\tilde{v}_y\rangle\approx 0$, one has in a linear shear flow still a nonvanishing positional cross-correlation $\langle\tilde{x}\tilde{y}\rangle=\dot{\gamma}\tau_p\langle\tilde{y}^2\rangle/2$. Its magnitude is determined by the shear rate $\dot{\gamma}$ and the noise strength via $\langle\tilde{y}^2\rangle$. According to this behavior and because $\langle\tilde{x}^2\rangle\neq\langle\tilde{y}^2\rangle$, we expect an anisotropic distribution of the positional fluctuations $\mathcal{P}(\tilde{\mathbf{r}})$, as sketched in Fig. 1 and as discussed below. For $f_{xy}\neq 0$ the anisotropy of the positional distribution has an additional contribution that depends on the magnitude of f_{xy}.

During the rest of the present Sec. IV A inertia effects are neglected and in addition, we assume an isotropic noise distribution with $f_{xy}=f_{yx}=0$ and $f_{xx}=f_{yy}=f_{zz}=2k_BT\zeta$. Both are good approximations for many experiments focusing on leading order effects of a shear flow on the fluctuations of particles. Taking into account the time dependence of the positional fluctuations, as given by Eq. (11), one obtains in terms of the dimensionless Weissenberg number,

$$\mathrm{Wi}=\tau_p\dot{\gamma}, \tag{34}$$

and the Heaviside step function $\Theta(t)$ the following time-dependent correlations:

$$\langle\tilde{x}(t)\tilde{x}(0)\rangle=\frac{k_BT}{k}\left[1+\frac{\mathrm{Wi}^2}{2}\left(1+\frac{|t|}{\tau_p}\right)\right]e^{-|t|/\tau_p}, \tag{35a}$$

$$\langle\tilde{y}(t)\tilde{y}(0)\rangle=\langle\tilde{z}(t)\tilde{z}(0)\rangle=\frac{k_BT}{k}e^{-|t|/\tau_p}, \tag{35b}$$

$$\langle\tilde{x}(t)\tilde{y}(0)\rangle=\frac{k_BT}{k}\frac{\mathrm{Wi}}{2}\left(1+2\frac{t}{\tau_p}\Theta(t)\right)e^{-|t|/\tau_p}. \tag{35c}$$

The cross-correlation between fluctuations along orthogonal directions, as given by the last equation, is shear induced and its asymmetry $\langle\tilde{x}(t)\tilde{y}(0)\rangle\neq\langle\tilde{x}(0)\tilde{y}(t)\rangle$ with respect to time reflection $t\rightarrow -t$ is one of the important effects of shear flow on the distribution of fluctuations.

For $t>0$, the algebraic prefactor in Eq. (35c) illustrates that a fluctuation $\tilde{y}(0)\neq 0$ of a particle is carried away by the flow along the x direction before the initial displacement starts to relax remarkably. This leads, during an initial period of time shorter than the relaxation time τ_p, to the growth of $\langle\tilde{x}(t)\tilde{y}(0)\rangle$, while $\langle\tilde{x}(0)\tilde{y}(t)\rangle$ decays monotonically (solid line in Fig. 2 corresponding to $t<0$). The predicted elementary signatures for the shear-induced cross-correlations, as shown in Fig. 2, are in agreement with experimental data as described recently in Ref. [15]. The expression $\langle\tilde{x}(t)\tilde{y}(0)\rangle$ is proportional to the Weissenberg number and takes its maximum at half of the particle's relaxation time $t_{max}=\tau_p/2$. For the correlations of the velocity fluctuations of the fluid in orthogonal directions a similar signature as in Eq. (35c) has been found [13], where however the mechanism is slightly different.

A comparison of the absolute values of the particle's fluctuations with experimental results may be difficult. However, one obtains from Eq. (35) and in terms of the dimensionless

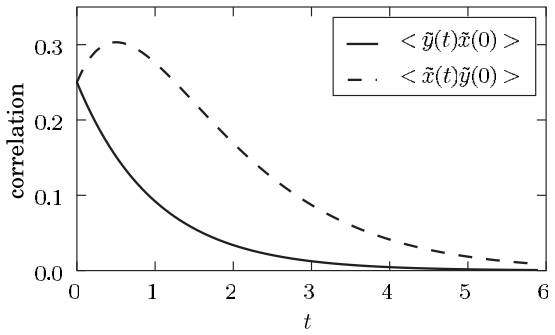

FIG. 2. Time dependence of the shear-induced cross-correlations $\langle \tilde{x}(t)\tilde{y}(0)\rangle$ (dashed line) and $\langle \tilde{x}(0)\tilde{y}(t)\rangle$ (solid line) as given by Eq. (35c) for the Weissenberg number Wi=1 and the relaxation time $\tau_p=1$.

Weissenberg number the following normalized ratios of the static correlations

$$\frac{\langle \tilde{x}(0)\tilde{y}(0)\rangle}{\langle \tilde{y}(0)\tilde{y}(0)\rangle} = \frac{\mathrm{Wi}}{2}, \tag{36a}$$

$$\frac{\langle \tilde{x}(0)\tilde{y}(0)\rangle}{\langle \tilde{x}(0)\tilde{x}(0)\rangle} = \frac{\mathrm{Wi}/2}{1+\mathrm{Wi}^2/2}. \tag{36b}$$

The left hand side and the right-hand side of Eq. (36) can be measured independently in different experiments and the results can be compared afterwards.

An anisotropic distribution of the particle's velocity $\mathcal{P}(\tilde{\mathbf{v}})$, as given by Eq. (26), is only obtained in the case of a finite cross-correlation f_{xy} of the stochastic forces. In contrast to this, the particle's distribution $\mathcal{P}(\tilde{\mathbf{r}})$ has in the overdamped limit an elliptical shape in the xy plane, even for a vanishing cross-correlation magnitude $f_{xy}=0$. In this limit an elliptical distribution $\mathcal{P}(\tilde{\mathbf{r}})$ is shown in Fig. 3 for the Weissenberg number Wi=2 and the relaxation time $\tau_p=1$. In Fig. 3 the time evolution of the particle's position, obtained by simulations of the basic Eq. (8), is plotted at equidistant times. This positional distribution can be characterized by the angle ϕ_p of the ellipsoid and the ratio V_p of its principal axis. The general expressions for ϕ_p and V_p, as given by Eqs. (24) and

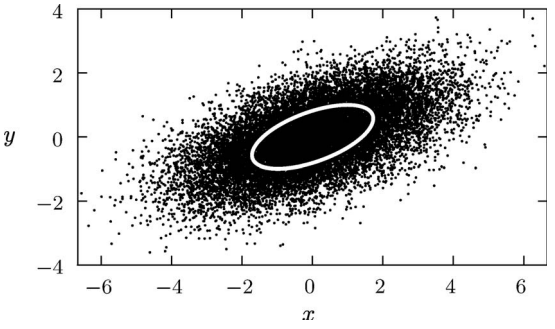

FIG. 3. Positional distribution of a particle in a harmonic potential with its minimum at $\mathbf{r}_0=(0,0,0)$ and exposed to a linear shear flow, as obtained by a stochastic simulation of the Eq. (8) in the overdamped limit for the Weissenberg number Wi=2 and the relaxation time $\tau_p=1$.

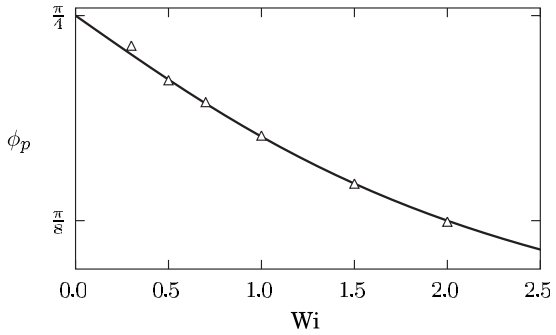

FIG. 4. The angle of the ellipse in the xy plane with respect to the flow lines as a function of the Weissenberg number Wi, as it is given by Eq. (37a). The triangles are the result of a simulation of Eq. (8) in the overdamped limit.

(25), can be further simplified in the case of a linear shear flow to functions of the dimensionless Weissenberg number Wi only

$$\tan\phi_p = \frac{1}{2}[\sqrt{4+\mathrm{Wi}^2}-\mathrm{Wi}], \tag{37a}$$

$$V_p = \left(\frac{\sqrt{4+\mathrm{Wi}^2}-\mathrm{Wi}}{\sqrt{4+\mathrm{Wi}^2}+\mathrm{Wi}}\right)^{1/2}. \tag{37b}$$

The two expressions in Eq. (37) suggest measurements of the shear-induced particle fluctuation effects, which are complementary to the measured static correlations. In experiments the particle positions may be recorded at equidistant times. By plotting these subsequent particle positions in the shear plane, a similar distribution is expected as shown by our numerical simulation in Fig. 3. From such an experimentally measured distribution for different shear rates the angle ϕ_p and the ratio between the principal axes, V_p, may be determined. If the determination of the Weissenberg number Wi is difficult or if the precision is not sufficient Eqs. (36) and (37) allow a consistency check between different aspects of the particle fluctuations, without a separate measurement of Wi. A cross-check has recently been performed in an experiment in which a good agreement between both approaches has been found, cf. Ref. [15].

In the limit of a vanishing Weissenberg number, $\mathrm{Wi}\to 0$, the angle ϕ_p of the ellipsoidal particle's distribution tends to $\phi_p=\pi/4$ and the positional variance becomes isotropic, $\langle\tilde{x}^2\rangle=\langle\tilde{y}^2\rangle$, corresponding to the ratio $V_p=1$. This trend is similar to the dependence of the orientation of vesicles in shear flow [57] or to the local orientation of the order parameter of nematic liquid crystals in plane shear flows [58].

If $\dot{\gamma}$ and therefore Wi is increased, the angle ϕ_p between the longer semiaxis and the x axis as well as the ratio V_p will decrease as shown in Figs. 4 and 5. The triangles in those figures have been obtained by numerical simulations of Eq. (8) for the same values of the Weissenberg number as used for the analytical curves. In our simulations of the Langevin model we have assumed an isotropic and Gaussian distributed white noise and vanishing cross-correlations $f_{xy}=0$. The simulation results confirm the assumption of a Gaussian dis-

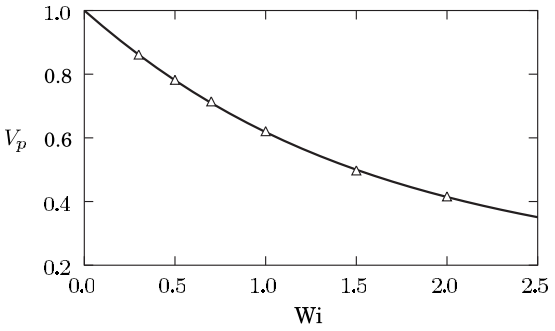

FIG. 5. The ratio V_p of the principal axis of the ellipse in Eq. (37b), as a function of the Weissenberg number Wi. The triangles are the result of a simulation of Eq. (8) in the overdamped limit.

tribution of the particle positions in the case of a shear flow in Sec. III. The analytical and numerical results on ϕ_p and V_p in Figs. 4 and 5 are in good agreement.

B. Plane Poiseuille flow

A Brownian particle is trapped by a harmonic potential close to $\mathbf{r}_0=(0,y_0,0)$ and exposed to a plane Poiseuille flow along the x direction,

$$\mathbf{u}(y) = u_p\left(1-\frac{y^2}{l^2}\right)\hat{\mathbf{e}}_x. \tag{38}$$

The particle fluctuations $\tilde{x}$ and $\tilde{y}$ describe deviations with respect to the mean values y_0 and $\langle x\rangle$, which is not zero as determined below. The flow velocity along the x direction may be expressed for further analysis in terms of the fluctuations $\tilde{y}$ as follows

$$u_x(\tilde{y}) = u_p\left(1-\frac{y_0^2}{l^2}\right) - 2\frac{u_p y_0}{l^2}\tilde{y} - \frac{u_p}{l^2}\tilde{y}^2. \tag{39}$$

Comparing this expression with Eq. (1) the coefficients in the latter equation are given by

$$c = -\chi := -\frac{u_p}{l^2},$$

$$a = u_p - \chi y_0^2,$$

$$b = -2\chi y_0. \tag{40}$$

Here χ describes the second derivative of the velocity profile, b the local shear rate and

$$\mathrm{Wi}(y_0) := -2\tau_p\chi y_0, \tag{41}$$

the local Weissenberg number $\mathrm{Wi}(y_0)$. With these identifications the elements of the covariance matrix C are again given via the expressions in Eq. (18) in terms of the strength of the noise, f_{xx}, f_{xy}, f_{yy}, and f_{zz} and the flow parameters.

The mean position of the particle in a plane Poiseuille flow can be determined via Eq. (12)

$$\langle x\rangle = \tau_p\left[u_p - \chi\left(y_0^2+\frac{1}{3}R^2\right) - \chi\langle\tilde{y}^2\rangle\right]. \tag{42}$$

In contrast to a linear shear flow, it includes a contribution depending on the particle's radius R, which is a pure deterministic effect due to Faxén's theorem [2,51]. The last term on the right-hand side describes an additional shift based on the positional variance $\langle\tilde{y}^2\rangle$ in the y direction. Both contributions are proportional to the second derivative χ of the flow profile and are therefore not present in linear shear flows.

In experiments Eq. (42) may be used to measure the spatial variation in the flow profile by detecting the mean displacement of a particle of radius R out of the optical tweezer potential. For such a measurement usually deterministic formulas are used to describe the relation between the displacement and the flow velocity. But Eq. (42) indicates that a correction due to thermal motion has to be taken into account.

The relations given by Eq. (18) relate the fluctuations of the velocity and the position of a particle to the externally controlled flow properties and the magnitudes of the thermal fluctuations. Consequently they allow, in a similar manner as to the linear shear flow, a determination of the magnitudes of the stochastic forces in terms of the measured covariances of the particle fluctuations

$$f_{yy} = 2k\zeta\langle\tilde{y}^2\rangle, \tag{43a}$$

$$f_{xy} = 2k\zeta\left(\langle\tilde{x}\tilde{y}\rangle - \frac{1}{2}\mathrm{Wi}(y_0)\langle\tilde{y}^2\rangle\right), \tag{43b}$$

$$f_{xx} = 2k\zeta\left(\langle\tilde{x}^2\rangle - \frac{1}{2}\frac{\mathrm{Wi}(y_0)}{\tau_p\omega^2}\langle\tilde{y}^2\rangle - \frac{2}{3}\tau_p^2\chi^2\left(\frac{5+2\tau_p^2\omega^2}{1+2\tau_p^2\omega^2}\right)\langle\tilde{y}^2\rangle^2 - \mathrm{Wi}(y_0)\langle\tilde{x}\tilde{y}\rangle\right). \tag{43c}$$

The difference compared to Eq. (33) is an additional contribution to f_{xx}, which depends on the second derivative of the Poiseuille flow. Further comments made above for a linear shear flow hold as well.

Similar to the end of the previous Sec. IV A, we neglect from here on the particle inertia and we assume in addition isotropically distributed noise with $f_{xy}=0$ and $f_{ii}=2k_BT\zeta$. The static correlations of the particle's positional fluctuations in the shear plane, given by Eq. (18), then reduce to

$$\langle\tilde{x}^2\rangle = \frac{k_BT}{k}\left(1+\frac{1}{2}\mathrm{Wi}(y_0)^2+\frac{2}{3}\chi^2\tau_p^2\frac{k_BT}{k}\right), \tag{44a}$$

$$\langle\tilde{y}^2\rangle = \frac{k_BT}{k}, \tag{44b}$$

$$\langle\tilde{x}\tilde{y}\rangle = \langle\tilde{y}\tilde{x}\rangle = \frac{k_BT}{k}\frac{\mathrm{Wi}(y_0)}{2}. \tag{44c}$$

The static cross-correlation $\langle\tilde{x}\tilde{y}\rangle$ has the same dependence on the Weissenberg number as in the linear shear case Eq. (35c) at $t=0$, if the local shear rate of the Poiseuille flow at the

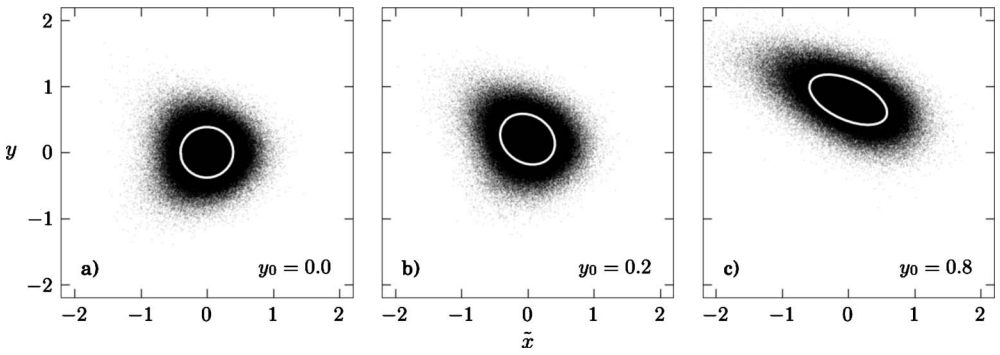

FIG. 6. Positional distribution of a Brownian particle in the xy plane captured by a harmonic potential with its minimum at $x_0=z_0=0$ and for different values of y_0. The particle is exposed to a Poiseuille flow and its dynamics have been calculated by stochastic simulations of the Eq. (8) in the overdamped limit for $\chi=1$, $k_BT=0.1$, and $\tau_p=1$.

potential center is taken. In contrast to a linear shear flow profile, the mean-square displacement of the particle in x direction, given by Eq. (44a), includes an additional constant contribution, $G:=2/3(\chi\tau_p k_B T/k)^2$, which is independent of the position of the potential minimum in the Poiseuille flow and therefore also independent of the local Weissenberg number. Besides the dependence on the second derivative χ of the flow profile, the contribution G is a direct function of the fluid temperature. Due to this contribution in Eq. (44a) one has $\langle\tilde{x}^2\rangle \neq \langle\tilde{y}^2\rangle$ and the isotropy of the particle's positional distribution in the shear plane is broken. This broken rotational symmetry also changes the analytically determined distribution function in Sec. III B along with the correlation matrix C_{ij} for a Poiseuille flow.

In addition to the calculations, we have performed simulations of the particle dynamics where we used isotropic and Gaussian distributed white noise in the overdamped version of Eq. (8). The resulting distributions for the particle's position are shown in Fig. 6 for three different positions y_0 of the potential center. With the potential minimum at the center of the flow ($y_0=0$) the numerical results show a broken mirror symmetry in x direction of the particle's positional distribution, cf. Fig. 6(a). One recognizes a parachute shape that is similar to the well-known conformation of vesicles and red blood cells in the center of a Poiseuille flow [59]. If one now makes the heuristic assumption of a Gaussian distribution for the particle's position in the case of a Poiseuille flow, as in Sec. III, but with the correlation matrix C_{ij} determined in terms of the Poiseuille flow parameters, one expects for the parameters in Fig. 6(a) an elliptical shape of the particle distribution. Indeed, the ratio between the principal axis in Fig. 6(a) is slightly smaller than 1.0. But within this analytical approximation, the $\pm x$ symmetry is not broken, which indicates the limitation of the heuristic approach.

Away from the center of the Poiseuille flow, for finite values of $y_0 \neq 0$, the $\pm y$ symmetry of the particle's positional distribution is also broken, as shown in Figs. 6(b) and 6(c). With increasing values of y_0 the local shear rate acting on the particle increases as well as the local Weissenberg number $\mathrm{Wi}(y_0)$. Consequently the cross-correlation $\langle\tilde{x}\tilde{y}\rangle$ in Eq. (44c) becomes nonzero and the particle's positional distribution in the xy plane approaches, according to our analytical results, an elliptic shape as indicated by the ellipses in Figs. 6(b) and 6(c). Again the full numerical simulations show deviations from the elliptical shape.

However, the inclination of the distribution and the inclination of the analytically determined ellipses agree rather well and therefore a determination of the angle ϕ_p for a Poiseuille flow according to Eq. (24), similar to that in the previous chapter, is reasonable and ϕ_p has the following form

$$\tan\phi_p = \frac{1}{2}\left[-\frac{y_0}{|y_0|}\sqrt{4+\left(\mathrm{Wi}(y_0)+\frac{4}{3}\frac{\tau_p^2\chi^2}{\mathrm{Wi}(y_0)}\langle\tilde{y}^2\rangle\right)^2} - \left(\mathrm{Wi}(y_0)+\frac{4}{3}\frac{\tau_p^2\chi^2}{\mathrm{Wi}(y_0)}\langle\tilde{y}^2\rangle\right)\right]. \tag{45}$$

We have shown in Sec. IV A, how the angle ϕ_p and the ratio V_p depend on the Weissenberg number of the linear shear flow. Since the local shear rate in a Poiseuille flow depends on the location y_0 of the minimum of the potential, one may plot ϕ_p and V_p [which is calculated via Eq. (25)] as a function of y_0 as shown in Fig. 7. Since the particle's distribution is anisotropic in the xy plane even for $y_0=0$, see Fig. 6(a), the corresponding principal axes are always unequal. This behavior is reflected in Fig. 7(b) where the inequality $V_p < 1$ holds for all values of y_0. The dependence of the angle ϕ_p on the local shear rate in a Poiseuille flow differs from the case of a linear shear flow: the function $\phi_p(y_0)$ is always well defined, even at the center of the flow, where it vanishes. This is one consequence of the asymmetry of the particle distribution. With increasing values of $|y_0|$ and therefore with increasing values of the local shear rate, the angle $|\phi_p|$ increases as well until it reaches some maximum value ϕ_{max} at $y_{0;max}$, as given by the following equations:

$$y_{0;max} = \pm\sqrt{\frac{\langle\tilde{y}^2\rangle}{3}}, \tag{46a}$$

$$\phi_{max} = \mp\arctan\left(\sqrt{1+\frac{4}{3}\tau_p^2\chi^2\langle\tilde{y}^2\rangle} - 2\tau_p\chi\sqrt{\frac{\langle\tilde{y}^2\rangle}{3}}\right). \tag{46b}$$

$y_{0,max}$ depends only on $\langle\tilde{y}^2\rangle$ and therefore on the width of the particle's distribution in y direction, which is determined by

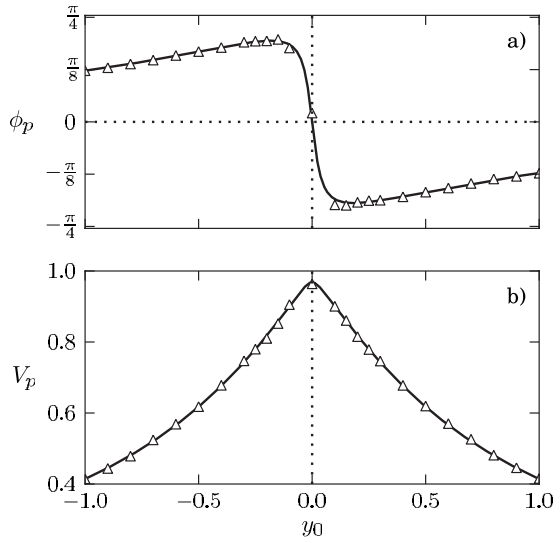

FIG. 7. The angle ϕ_p in the xy plane according to Eq. (45) is shown in (a) and the ratio V_p between the two principal axes, as determined by the Eq. (44) and Eq. (25), is shown in (b). Both are plotted as a function of the position of the potential minimum y_0 and for the parameters $\chi=\tau_p=1$, $\langle\tilde{y}^2\rangle=k_BT/k=0.1$. The triangles are the result of simulations of the Eq. (8) with the same parameter set.

the ratio between the thermal energy and the spring constant related to the harmonic potential acting on the particle. Increasing $|y_0|$ beyond $|y_{0,max}|$ the local shear rate, $\mathrm{Wi}(y_0)$, increases too, but ϕ_p starts to decrease; a similar behavior as seen in Sec. IV A. In the range $|y_0|>|y_{0,max}|$ the local shear dominates the curvature effects more and more and the Poiseuille flow resembles a linear shear flow. In addition, the particle's distribution approaches an ellipse as obtained by the heuristic approximation. As mentioned above, the heuristic analytical approach becomes exact in the case of a linear shear flow.

In Fig. 7 the analytical results on ϕ_p and V_p have been compared with our numerical simulations. In spite of the fact that we assumed for our analytical calculations a Gaussian distribution of the positional fluctuations $\tilde{x}$ and $\tilde{y}$, the results show surprisingly good agreement. The major reason for this good agreement is that we calculated the inertia tensor for the particle distribution, which includes only second order moments as assumed for the Gaussian distribution.

C. Pipe flow

For a flow profile in a pipe of radius d, cylindrical polar coordinates are appropriate. Similar to a plane Poiseuille flow the dependence of the velocity profile on the radial position ρ is also quadratic. Consequently, the ρ dependence corresponds now to the y dependence in the case of the plane Poiseuille flow. The velocity profile for the pipe flow, where the pipe axis coincides with the x axis, is of the following form,

$$u_x = u_p\left(1-\frac{\rho^2}{d^2}\right). \tag{47}$$

The results described above in Sec. IV B apply qualitatively also for the pipe flow.

With the potential minimum located at ρ_0 the coefficients in the Eq. (1) are $a=u_p(1-\frac{\rho_0^2}{d^2})$, $c=-\chi:=-\frac{u_p}{d^2}$, and $b=2\rho_0 c$. Moreover, one has to consider $\bar{a}=a+\frac{2}{3}R^2c$ in Eq. (5). The major difference to the plane Poiseuille flow is the prefactor $\frac{2}{3}$ instead of $\frac{1}{3}$. This is a consequence of the $2D$ Laplacian instead of a $1D$ second derivative in Eq. (4). The mean position of the particle is in terms of the pipe flow of the following form

$$\langle x\rangle = u_p\tau_p - \chi\tau_p\left(y_0^2+\frac{2}{3}R^2\right) - \chi\tau_p\langle y^2\rangle. \tag{48}$$

Besides the factor 2 in front of R^2 this expression corresponds to that in Eq. (42).

V. CONCLUSION

In this work, we have calculated analytically and numerically the autocorrelations and cross-correlations between different components of the velocity and the positional fluctuations of a Brownian particle in a harmonic potential, which is exposed to different shear flows. In addition, the particle's probability distribution in the harmonic potential has been determined as a function of the flow parameters. By solving an appropriate Langevin model, cross-correlations between velocity and positional fluctuations along orthogonal directions have been found and several suggestions for experimental measurements are made.

Cross-correlations between orthogonal velocity components occur only if there is already a cross-correlation between stochastic forces along orthogonal directions in the related Langevin model. On the other hand, we find cross-correlations between particle fluctuations along orthogonal directions without cross-correlations of orthogonal stochastic force components and their magnitude increases with the dimensionless shear rate, the Weissenberg number.

There are recent calculations on shear-induced cross-correlations between orthogonal fluctuations of freely floating particles [16,18]. They have the same origin as those discussed in this work. However, while measurements of the shear-induced cross-correlations of freely moving particles may be difficult, shear-induced cross-correlations for particles in a potential can be measured in a controlled manner. This insight was the basis of recent successful measurements on the cross-correlations between particle fluctuations along orthogonal directions as described in Ref. [15]. In this experiment, harmonic potentials for small latex spheres are induced by optical tweezers. The particle is simultaneously exposed to a linear shear flow in a special flow cell and its Brownian motion is investigated directly. In the same experiment and in a forthcoming work, the cross-correlations and anticorrelations between two particles captured in two neighboring potentials and exposed to shear flows are also investigated.

The measurements on the positional cross-correlation, $\langle x(t)y(0)\rangle$, presented in Ref. [15], exhibit a similar maximum as predicted by the expression in Eq. (35c) and as shown in Fig. 2. This maximum is a typical signature of Brownian motion in shear flow and it is found where the shear rate

approximately equals half of the particle's relaxation time. Also the elliptic shape of the particle's distribution, $P(\mathbf{r})$, as shown in Fig. 3, has been measured in Ref. [15]. The angle ϕ_p, enclosed by the major axis of the distribution $P(\mathbf{r})$ and the ratio V_p between the length of the two principal axes on the one hand and the magnitude of the static correlations on the other hand focus on different aspects of the dynamics of a particle in a potential exposed to a shear flow. The interrelation between these different aspects of the Brownian particle dynamics can be used for consistency checks in experiments; such cross-checks are described Ref. [15] for the case of a linear shear flow. They are also possible in experiments with Poiseuille flow as forthcoming measurements may demonstrate.

Shear-induced correlations of fluctuations of the fluid velocity with respect to a linear shear flow were found theoretically [13,14]. They are traced back to the non-normal property of the Navier-Stokes equation linearized around the linear shear profile [13] and these velocity fluctuations play an important role in a shear flow for its instability and the onset of turbulence. The cross-correlations between these velocity fluctuations exhibit a similar extremum as given by Eq. (35c), but it is a slightly different mechanism leading to this similar behavior on the level of the correlation function. This interrelation may be discussed in more detail in future work.

Stochastic forces acting on a particle in a fluid are caused by the velocity fluctuations of the fluid surrounding a particle. In quiescent fluids the correlations for velocity fluctuations are isotropically distributed. For reasons of simplicity, this is quite often assumed in models to investigate the Brownian motion of particles in shear flow. In that case, cross-correlations between stochastic forces along orthogonal directions vanish in the Langevin equation of motion. Shear-induced cross-correlations between orthogonal components of fluctuations of the fluid velocity are indeed small compared to the shear independent contributions [14,23] and hence this simplification is reasonable. However, to which extent such cross-correlations of the fluid velocity may quantitatively modify the presented results on the cross-correlations of particle displacements need further investigations.

In numerical simulations of the dynamics of a Brownian particle in a potential and exposed to a Poiseuille flow we found higher order correlations for the particle fluctuations of non-Gaussian behavior. However, for deriving our analytical results on the angle ϕ_p, which the major axis of the particle distribution encloses with the flow direction, and the ratio V_p between the lengths of the two principal axes, we assumed Gaussian distributed particle fluctuations also in Poiseuille flow. Accordingly, a perfect agreement between the results of the numerical simulations and the analytical calculations on ϕ_p and V_p could not be expected. Nevertheless, we find good agreement between both approaches, cf. Fig. 7, especially further away from the center of the Poiseuille flow, where the linear contribution in the flow profile dominates and where the assumptions are better fulfilled.

ACKNOWLEDGMENTS

We would like to thank A. Ziehl and C. Wagner for inspiring discussions. This work was supported by the German science foundation via the priority program on microfluids and nanofluidics Grant No. SPP 1164 and via the research unit Grant No. FOR 608.

APPENDIX A: CROSS-CORRELATION $\langle \tilde{v}_x(t)\tilde{v}_y(t)\rangle$

In this appendix, we discuss the correlation $\langle \tilde{v}_x(t)\tilde{v}_y(t)\rangle$ and we show that it includes, besides the contribution $\propto f_{xy}$ in Eq. (18c), in the limit $k\to 0$ an additional contribution $\propto f_{yy}$, which corresponds to the result described in Ref. [18] from Eq. (11) one obtains

$$\tilde{v}_x(t) = \int_0^t d\tau a_{vv}(t-\tau)\left[\frac{F_x^b(\tau)}{m} + 2\beta b\tilde{y}(\tau)\right], \tag{A1}$$

$$\tilde{v}_y(t) = \int_0^t d\tau a_{vv}(t-\tau)\frac{F_y^b(\tau)}{m}, \tag{A2}$$

$$\tilde{y}(\tau) = \int_0^t d\tau' a_{rv}(\tau-\tau')\frac{F_y^b(\tau)}{m}, \tag{A3}$$

with the abbreviations

$$a_{vv}(t) = \hat{\mathbf{e}}_v^T e^{\mathrm{L}(t)}\hat{\mathbf{e}}_v, \tag{A4}$$

$$a_{rv}(t) = \hat{\mathbf{e}}_r^T e^{\mathrm{L}(t)}\hat{\mathbf{e}}_v \quad \text{with} \quad \hat{\mathbf{e}}_r = \begin{pmatrix}1\\0\end{pmatrix}. \tag{A5}$$

The equal-time velocity correlation takes then the form

$$\begin{aligned}\langle \tilde{v}_x(t)\tilde{v}_y(t)\rangle = &\int_0^t d\tau\int_0^t d\tau' a_{vv}(t-\tau)a_{vv}(t-\tau')\\ &\times\left\langle\frac{F_x^b(\tau)F_y^b(\tau')}{m^2}\right\rangle + 2\beta b\int_0^t d\tau a_{vv}(t-\tau)\\ &\times\langle\tilde{y}(\tau)\tilde{v}_y(t)\rangle.\end{aligned} \tag{A6}$$

With the correlation between the position $\tilde{y}(t)$ and the velocity $\tilde{v}_y(t)$,

$$\langle\tilde{y}(\tau)\tilde{v}_y(t)\rangle = \frac{f_{yy}}{m^2}\int_0^{min(t,\tau)} d\tau'' a_{rv}(\tau-\tau'')a_{vv}(t-\tau''), \tag{A7}$$

one ends up with the expression

$$\begin{aligned}\langle \tilde{v}_x(t)\tilde{v}_y(t)\rangle &= \frac{f_{xy}}{m^2}\int_0^t d\tau a_{vv}(t-\tau)^2\\ &+ 2\beta b\frac{f_{yy}}{m^2}\int_0^t d\tau\int_0^\tau d\tilde{\tau} a_{vv}(t-\tau)a_{rv}(\tau-\tilde{\tau})a_{vv}(t-\tilde{\tau})\\ &= \frac{f_{xy}}{m^2}\frac{G_1(t)}{2} + 2\beta b\frac{f_{yy}}{m^2}\frac{G_2(t)}{4},\end{aligned} \tag{A8}$$

where we have introduced the functions $G_1(t)$ and $G_2(t)$ as well as the parameter δ

$$G_1(t) = \left[\frac{\beta \cos^2(\delta t)}{\delta^2} + \frac{\cos(\delta t)\sin(\delta t)}{\delta} - \frac{\delta^2 + 2\beta^2}{2\delta^2 \beta} \right] e^{-2\beta t} + \frac{1}{2\beta}, \tag{A9}$$

$$G_2(t) = \left[\frac{\sin(\delta t)\cos(\delta t)}{2\delta^3} - \frac{\beta \sin^2(\delta t)}{\delta^4} + \frac{t \sin^2(\delta t)}{2\delta^2} + \frac{\beta t \cos(\delta t)\sin(\delta t)}{\delta^3} - \frac{t \cos^2(\delta t)}{2\delta^2} \right] e^{-2\beta t}, \tag{A10}$$

$$\delta = \sqrt{\omega^2 - \beta^2}. \tag{A11}$$

In the limit $t \to \infty$ the contribution $G_1(t)$ remains finite, $\lim_{t\to\infty} G_1(t) = \frac{1}{2\beta}$. For finite values of $\tau_p = \zeta/k$ the function $G_2(t)$ vanishes on a time scale $t \gg 1/(2\beta)$ too. But in the limit of a vanishing laser tweezer potential, $k \sim \omega^2 \to 0$, one has $\delta \simeq \pm i[\beta - \omega^2/(2\beta) + \ldots]$ and in this limit some contributions of $G_2(t)$ cancel each other and the remaining terms are proportional to $\exp(-2t/\tau_p)$. These contributions do not decay in the limit $\tau_p \to \infty$ and one gets $G_2(t) = 1/(8\beta^3)$. In this case one obtains even for $f_{xy} = 0$ a nonzero cross-correlation $\langle \tilde{v}_x(t)\tilde{v}_y(t)\rangle = \frac{b f_{yy}}{4\zeta^2}$, which is exactly the same result as described in [18].

APPENDIX B: ANISOTROPIC TRAP

In experiments the force exerted by the optical tweezer on a colloidal particle may be anisotropic in the shear plane. For instance, the force constant may be different along and perpendicular to the laser beam. If the laser beam does not hit the shear plane perpendicularly the difference between the force constants in x and y direction increases with the deviation from the orthogonal direction to the shear plane. Let's assume in Eq. (3) a different force constant for each direction: k_x, k_y, and k_z.

The relaxation of the particle is now different along different directions around the potential minimum. In order to take this effect into account, we introduce three relaxation times in the same way as in Sec. III,

$$\tau_{p;i} = \frac{2\beta}{\omega_i^2} = \frac{\zeta}{k_i}, \tag{B1}$$

and we further define the fraction

$$\mu := \frac{\omega_y}{\omega_x} = \frac{k_y}{k_x}. \tag{B2}$$

between the eigenfrequencies in the shear plane, which is used to express k_y by k_x via $k_y = \mu k_x$.

The covariance matrix C from Sec. III depends now in a complex manner on the different force constants, but in the limit $\mu \to 1$ and $k_z = k_x$ the result from the previous sections are obtained again.

The different static correlations as given for the isotropic forces in Sec. III change as follows:

$$\langle \tilde{v}_y^2 \rangle = \frac{1}{4} \frac{f_{yy}}{m^2 \beta}, \tag{B3}$$

$$\langle \tilde{y}^2 \rangle = \frac{1}{4} \frac{f_{yy}}{m^2 \beta \omega_y^2} = \frac{\langle \tilde{v}_y^2 \rangle}{\omega_y^2}, \tag{B4}$$

$$\langle \tilde{v}_x^2 \rangle = \frac{1}{4} \frac{f_{xx}}{m^2 \beta} + \frac{1}{2} b^2 \langle \tilde{y}^2 \rangle \Theta_1 + \frac{8}{3} c^2 \frac{\omega_x^2 \tau_{p;x}^2}{(1 + 2\tau_{p;x}^2 \omega_x^2)} \langle \tilde{y}^2 \rangle^2 \Theta_2 - b \frac{1 - \mu^2}{1 + \mu^2} \frac{2\langle \tilde{v}_x \tilde{v}_y \rangle}{\tau_{p;x} \omega_x^2}, \tag{B5}$$

$$\langle \tilde{x}^2 \rangle = \frac{\langle \tilde{v}_x^2 \rangle}{\omega_x^2} + \frac{1}{2} \tau_{p;x}^2 b^2 \langle \tilde{y}^2 \rangle \Pi_1 + \frac{2}{3} \tau_{p;x}^2 c^2 \langle \tilde{y}^2 \rangle^2 \Pi_2 + b \tau_{p;x} \frac{2\langle \tilde{v}_x \tilde{v}_y \rangle}{\omega_x^2 (1 + \mu^2)}, \tag{B6}$$

$$\langle \tilde{v}_z^2 \rangle = \frac{1}{4} \frac{f_{zz}}{m^2 \beta}, \tag{B7}$$

$$\langle \tilde{z}^2 \rangle = \frac{1}{4} \frac{f_{zz}}{m^2 \beta \omega_y^2} = \frac{\langle \tilde{v}_z^2 \rangle}{\omega_z^2}, \tag{B8}$$

where the following abbreviations have been introduced:

$$\Theta_1 = 2 \frac{\mu^2}{1 + \mu^2},$$

$$\Theta_2 = 3\mu^2 \frac{\tau_{p;x}^2 \omega_x^2 + \frac{1}{6}(1 + 2\mu^2)}{(1 + 2\mu^2)\tau_{p;x}^2 \omega_x^2 + \frac{1}{6}(1 - 4\mu^2)^2},$$

$$\Pi_1 = 2 \frac{(1 + \mu^2)^2 + \frac{(1 - \mu^2)(1 + 2\mu^2)}{\tau_{p;x}^2 \omega_x^2} + \frac{1}{4} \frac{(1 - \mu^2)^3}{\tau_{p;x}^4 \omega_x^4}}{(1 + \mu^2)\left((1 + \mu^2) + \frac{1}{2} \frac{1}{\tau_{p;x}^2 \omega_x^2} (1 - \mu^2)^2 \right)^2},$$

$$\Pi_2 = \frac{1 + \frac{1}{3} \frac{1}{\tau_{p;x}^2 \omega_x^2} (2 + \mu^2) + \frac{1}{12} \frac{1}{\tau_{p;x}^4 \omega_x^4} (1 - 2\mu^2)(1 - 4\mu^2)}{1 + \frac{1}{2} \frac{1}{\tau_{p;x}^2 \omega_x^2} \left(\frac{(1 + 2\mu^2)}{3} + \frac{1}{2} \frac{1}{\tau_{p;x}^2 \omega_x^2} \frac{(1 - 4\mu^2)^2}{9} \right)}.$$

Since the y and z displacements are independent of any other direction, as can be seen in Eq. (11), their autocorrelations are functions of the individual force constant only and do not depend on μ. However, the autocorrelations for the velocity and the position in x direction depends in a complex manner on the different force constants. The same applies for the cross correlations in the shear plane as follows

$$\langle \tilde{v}_x \tilde{v}_y \rangle = \langle \tilde{v}_y \tilde{v}_x \rangle = \frac{1}{4} \frac{f_{xy}}{m^2 \beta} \frac{\tau_{p;x}^2 \omega_x^2 (1+\mu^2)}{\left[\tau_{p;x}^2 \omega_x^2 (1+\mu^2) + \frac{1}{2}(1-\mu^2)^2 \right]} + \frac{1}{4} b \langle \tilde{y}^2 \rangle \frac{\tau_{p;x} \omega_x^2 \mu^2 (1-\mu^2)}{\left[\tau_{p;x}^2 \omega_x^2 (1+\mu^2) + \frac{1}{2}(1-\mu^2)^2 \right]}, \quad \text{(B9)}$$

$$\langle \tilde{x}\tilde{y} \rangle = \langle \tilde{y}\tilde{x} \rangle = \left[\frac{\langle \tilde{v}_x \tilde{v}_y \rangle}{\omega_x^2} + \frac{1}{2} \tau_{p;x} b \langle \tilde{y}^2 \rangle \right] \frac{2}{(1+\mu^2)}, \quad \text{(B10)}$$

$$\langle \tilde{x}\tilde{v}_y \rangle = -\langle \tilde{y}\tilde{v}_x \rangle = -\frac{\mu^2 b \langle \tilde{y}^2 \rangle}{(1+\mu^2)} + \frac{(1-\mu^2)}{(1+\mu^2)} \frac{\langle \tilde{v}_x \tilde{v}_y \rangle}{\tau_{p;x} \omega_x^2}. \quad \text{(B11)}$$

[1] A. Einstein, Ann. Phys. **17**, 549 (1905).
[2] J. K. G. Dhont, *An Introduction to Dynamics of Colloids* (Elsevier, Amsterdam, 1996).
[3] H. Stone and S. Kim, AIChE J. **47**, 1250 (2001).
[4] J. Ottino and S. Wiggins, Philos. Trans. R. Soc. London, Ser. A **362**, 923 (2004).
[5] L. Holzer and W. Zimmermann, Phys. Rev. E **73**, 060801(R) (2006).
[6] C. Lutz, M. Reichert, H. Stark, and C. Bechinger, Europhys. Lett. **74**, 719 (2006).
[7] G. Taylor, Proc. R. Soc. London, Ser. A **219**, 186 (1953).
[8] A. Groisman and V. Steinberg, Nature (London) **410**, 905 (2001).
[9] T. Perkins, D. Smith, and S. Chu, Science **276**, 2016 (1997).
[10] P. G. deGennes, Science **276**, 1999 (1997).
[11] A. Groisman and V. Steinberg, Nature (London) **405**, 53 (2000).
[12] S. Grossmann, Rev. Mod. Phys. **72**, 603 (2000).
[13] B. Eckhardt and R. Pandit, Eur. Phys. J. B **33**, 373 (2003).
[14] G. Khujadze, M. Oberlack, and G. Chagelishvili, Phys. Rev. Lett. **97**, 034501 (2006).
[15] A. Ziehl, J. Bammert, L. Holzer, C. Wagner, and W. Zimmermann, Phys. Rev. Lett. **103**, 230602 (2009).
[16] K. Miyazaki and D. Bedeaux, Physica A **217**, 53 (1995).
[17] G. Subramanian and J. Brady, Physica A **334**, 343 (2004).
[18] Y. Drossinos and M. W. Reeks, Phys. Rev. E **71**, 031113 (2005).
[19] M. San Miguel and J. M. Sancho, Physica A **99**, 357 (1979).
[20] I. Santamaria-Holek, D. Reguera, and J. M. Rubi, Phys. Rev. E **63**, 051106 (2001).
[21] R. Foister and T. van de Ven, J. Fluid Mech. **96**, 105 (1980).
[22] G. Fuller, J. Rallison, R. Schmidt, and L. Leal, J. Fluid Mech. **100**, 555 (1980).
[23] L. Holzer, Ph. D thesis, Universität Bayreuth, 2009.
[24] M. Hoppenbrouwers and W. van de Water, Phys. Fluids **10**, 2128 (1998).
[25] D. G. Grier, Nature (London) **424**, 810 (2003).
[26] A. Ashkin, J. Dziedzic, J. Bjorkholm, and S. Chu, Opt. Lett. **11**, 288 (1986).
[27] S. Chu, Science **253**, 861 (1991).
[28] T. Perkins, S. Quake, D. Smith, and S. Chu, Science **264**, 822 (1994).
[29] T. Perkins, D. Smith, R. Larson, and S. Chu, Science **268**, 83 (1995).
[30] F. Brochard-Wyart, Europhys. Lett. **30**, 387 (1995).
[31] R. G. Larson, T. T. Perkins, D. E. Smith, and S. Chu, Phys. Rev. E **55**, 1794 (1997).
[32] R. Rzehak, D. Kienle, T. Kawakatsu, and W. Zimmermann, Europhys. Lett. **46**, 821 (1999).
[33] R. Rzehak, W. Kromen, T. Kawakatsu, and W. Zimmermann, Eur. Phys. J. E **2**, 3 (2000).
[34] D. Kienle and W. Zimmermann, Macromolecules **34**, 9173 (2001).
[35] R. Rzehak and W. Zimmermann, Europhys. Lett. **59**, 779 (2002).
[36] J. C. Meiners and S. R. Quake, Phys. Rev. Lett. **82**, 2211 (1999).
[37] S. Henderson, S. Mitchell, and P. Bartlett, Phys. Rev. Lett. **88**, 088302 (2002).
[38] E. Dufresne, D. Altman, and D. Grier, Europhys. Lett. **53**, 264 (2001).
[39] E. R. Dufresne, T. M. Squires, M. P. Brenner, and D. G. Grier, Phys. Rev. Lett. **85**, 3317 (2000).
[40] M. Atakhorrami, G. H. Koenderink, C. F. Schmidt, and F. C. MacKintosh, Phys. Rev. Lett. **95**, 208302 (2005).
[41] J. C. Crocker, M. T. Valentine, E. R. Weeks, T. Gisler, P. D. Kaplan, A. G. Yodh, and D. A. Weitz, Phys. Rev. Lett. **85**, 888 (2000).
[42] M. Polin, D. G. Grier, and S. Quake, Phys. Rev. Lett. **96**, 088101 (2006).
[43] P. T. Korda, M. B. Taylor, and D. G. Grier, Phys. Rev. Lett. **89**, 128301 (2002).
[44] J. Bammert, S. Schreiber, and W. Zimmermann, Phys. Rev. E **77**, 042102 (2008).
[45] J. Bammert and W. Zimmermann, Eur. Phys. J. E **28**, 331 (2009).
[46] M. P. MacDonald, G. C. Spalding, and K. Dholakia, Nature (London) **426**, 421 (2003).
[47] R. Simmons, J. Finer, S. Chu, and J. Spudich, Biophys. J. **70**, 1813 (1996).
[48] J. Crocker and D. Grier, J. Colloid Interface Sci. **179**, 298 (1996).
[49] L. D. Landau and E. M. Lifschitz, *Lehrbuch der Theoretischen Physik: Hydrodynamik*, 2nd ed. (Akademie Verlag, Berlin, 1987).
[50] G. G. Stokes, Trans. Cambridge Phil. Soc. **IX**, 8 (1850).
[51] H. Faxen, Z. Angew. Math. Mech. **7**, 79 (1927).
[52] L. E. Reichl, *A Modern Course in Statistical Physics*, 2nd ed. (Wiley, Berlin, 1998).
[53] L. D. Landau and E. M. Lifschitz, *Lehrbuch der Theoretischen Physik: Statistische Physik II* (Akademie Verlag, Berlin, 1980).
[54] N. G. van Kampen, *Stochastic Processes in Physics and Chemistry* (Elsevier, Amsterdam, 2004).
[55] B. Bamieh and M. Dahleh, Phys. Fluids **13**, 3258 (2001).

[56] J. M. Ortiz de Zárate and J. V. Sengers, Phys. Rev. E **77**, 026306 (2008).

[57] M. Kraus, W. Wintz, U. Seifert, and R. Lipowsky, Phys. Rev. Lett. **77**, 3685 (1996).

[58] P. G. deGennes and J. Prost, *The Physics of Liquid Crystals* (Clarendon Press, Oxford, 2006).

[59] G. Danker, P. M. Vlahovska, and C. Misbah, Phys. Rev. Lett. **102**, 148102 (2009).